

Impact of Design Dimension Optimization on Capacitive Sensor Performance for Particulate Matter Detection and Measurement



K. V. Kulkarni^{1*} and S. S. Chorage²

¹ Department of Electronics and Telecommunication Engineering, All India Shri Shivaji Memorial Society's Institute of Information Technology, Savitribai Phule Pune University, Pune, India..

² Department of Electronics and Telecommunication Engineering, Bharti Vidyapeeth's College of Engineering for Women, Savitribai Phule Pune University, Pune, India.



ABSTRACT: Particulate matter (PM) emissions from exhaust gases are major pollutants and cause serious health problems. Diesel particulate filters (DPF) are used for monitoring and trapping particulates from exhaust gases. For sensing these particulates sensors are used downstream of a DPF. The present study proposes an interdigitated electrode (IDE) capacitive sensor for detecting and measuring deposited particulates on the sensor surface. The sensor dimensions are optimized to detect and measure the least deposition of particulates. The paper presents improvement in sensor performance, a high selectivity of 65.70% with an accuracy of 87.26%. Dimension optimization extracts capacitance of 581 pF manifolds 10 times more than the reference sensor from the literature. The study presents a sensor with a thin sensing layer manufactured by optical lithography and a lift-off method for IDE. Measurements and testing showed that the sensor measures the lowest particulate mass of 0.0045 mg in 3.4 ms

KEYWORDS: Sensor optimization, Particulate sensing, Capacitive sensing, Optimization analysis, PM sensor

[Received Dec. 28, 2023; Revised May 25, 2024; Accepted July 2, 2024]

Print ISSN: 0189-9546 | Online ISSN: 2437-2110

I. INTRODUCTION

Heavy-duty vehicles produce and emit harmful gases because of incomplete combustion. The major content of these harmful emissions is carbon black, known as soot or particulate matter. These particulates are microscopic, varying from 10 nm to 100 nm, and cause adverse effects on human health having some mutagen effects. Particulates cannot be removed by any chemical method. The only way to remove or reduce the carbon black emissions to the environment is to burn or filter them (Deng et al, 2019). The literature frequently discusses four primary categories of particulate matter measurements, particle mass, number, surface area, and size distribution. Particle mass measurements help evaluate the health impact of particulate matter (Nagendra et al, 2021). The particulate filters help to reduce particulate contents in the emitted exhaust. In the literature particulate detection and measurement techniques are broadly classified as direct and indirect (Scott et al, 2019). The direct methods directly quantify the mass or volume of particulate matter within the filter. Indirect methods indirectly assess the amount of particulate matter accumulated in the diesel particulate filters (DPF) and alternatively, slip particulates from the exhaust gas. Indirect methods like sensing are preferred for their ability to provide continuous feedback without the need for intrusive, time-consuming sample collection and for ease of integration into vehicle control systems (Alexander et al, 2017). Direct measurement techniques offer more precise information

about the actual mass of particulate matter in the DPF. However, they may be less common in everyday automotive applications due to factors like cost, complexity, and the need for periodic removal for measurements. Figure 1 presents the broad classification of particulate detection methods (Alexander et al, 2017).

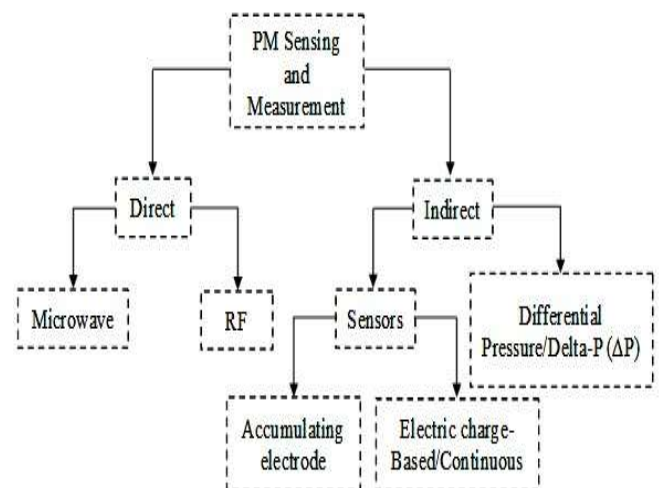


Figure 1: Methods for particulate detection and measurements.

A microwave-based technique (Markus et al, 2017) uses electrically conductive metallic filter housing to act as a cavity resonator for electromagnetic fields. An electric field
doi: <http://dx.doi.org/10.4314/njtd.v21i3.2260>

*Corresponding author: vaishsan2000@gmail.com

can be impressed into the housing with a stub antenna. Particulate accumulation in the field affects the field distribution by changing the overall electrical affecting S-parameters. The RF-based method utilized radio frequencies (RF) to directly monitor the state of the particulate filter. The RF signal propagates through the ceramic filter thereby providing a direct measurement of the filter's state (Sappok et al, 2013).

Conventional methods use an indirect approach utilizing filter pressure drop measurements, so-called delta-P sensors, to deduce the filter particulate matter (PM) load from the exhaust flow restriction due to the accumulated PM. For many reasons PM detection and measurement are challenging for pressure-based approaches. Hence particulate sensors have been developed to detect particulates that may pass through the particulate filter, as a result of a filter failure (Alexander et al, 2017). Different types of sensors are broadly defined as accumulating electrode sensors, and electric charge-based sensors (Sappok et al, 2013). The accumulating electrode-type sensors provide a time-averaged PM measurement. Charge-based system operates by inducing a charge on the incoming particulates and monitoring that charge to determine the particulate emissions. A conventional conductometric sensing principle measures an electrical current or resistance between two electrodes while particulates deposit on the electrodes. The orientation of the sensor greatly affects the results and needs to be addressed in future studies (Feulner et al, 2015). A resistive sensor is modified as a capacitive sensor for particulate detection built by covering the electrode area with an insulating, thin, and dense alumina layer. It can operate at higher collecting voltages reducing the blind time and influence of the temperature on the measurement signal than the conductometric sensor (Hagen et al, 2016). The noticed drawbacks of the device are a more complex setup and measuring small capacitance with high resolution. Even better results can be expected by an improved sensor design reducing line width and spaces of the electrode structure. This provides scope for further research focusing on technological aspects on the one side (Gunter et al, 2015). The key issues in sensing mechanisms are sensor design and performance evaluation. The geometry of the sensor electrodes decides the sensitivity distribution. An optimal sensor design needs a trade-off between different design parameters (Wuqiang Yang et al, 2010). The sensor's sensitivity is affected by the design parameters of capacitive interdigitated electrodes (IDEs). The IDE metal thickness directly affects the sensitivity (N. Salama et al, 2015). An overview of interdigital sensors and transducers, modelling techniques, and limitations was presented by (Alexander et al, 2004) focusing on geometric structure in various sensor and transducer designs known as interdigital electrodes.

Significant advantages of interdigital electrode structure include one-sided access to the material under test (MUT), the convenience of application of sensitive coatings, and the possibility of spectroscopy measurements. (Back et al, 2020) developed a capacitive sensor for real-time monitoring of nanoscale particulate matter in personal sampling devices for the mining environment. Limitations of some frequently

used design methods for microelectromechanical (MEMS) design optimization were analysed presenting evolutionary computation methods for the design optimization by (Wang et al, 2019).

The research aims to investigate the effect of capacitive sensor design optimization on its performance. The study presents the potential and scope for an optimized capacitive sensor to detect and measure particulate matter deposition (Hagen et al, 2016) with improved selectivity. The sensor modelling is simulated and executed in COMSOL Multiphysics software environment. The sensor is fabricated with optical lithography and a lift-off process for IDE and SiO₂ as substrate material. DC probe station and SEM (Scanning Electronic Microscopy) were used to characterize and investigate sensor performance. A gas calibration chamber is utilized to integrate the gas sensor and check for cross-sensitivity to present the selectivity. The paper comprises four sections. The first introduces the literature review and research contributions. The second focuses on the working principle of capacitive sensors. The third briefly outlines the methodology, and the fourth describes the results and discussions. This structure ensures a concise progression from literature to methodology and outcomes.

II. THEORETICAL ANALYSIS

A. Capacitive Sensing Principle

The capacitive particulate detection technique relies on capacitance variations measured by a pair of microelectrodes placed in the proximity of a stream of PM. The particulate (replaces the equivalent fraction of air dielectric with its volume) interacts with the electric field lines and increases the capacitance between the electrodes (Marco et al, 2014). The two main configurations, parallel and coplanar are shown in Figure 2(a) and 2(b) respectively. PM stream is forced to flow between the electrodes. The presence of particulates generates a capacitive jump (ΔC) whose amplitude is related to the diameter D and dielectric constant of the particulate.

The coplanar geometry has several advantages over the parallel-plate geometry like easier fabrication of electrodes, permitting particulate detection over a wide range of sizes, allowing the sensor to operate in two different conditions: when the PM flows over the electrodes, it allows taking advantage of the nonnegligible effect of gravity on the particulate enabling significant relaxation of the detection speed requirements. The largest PM diameter determines the distance between the plates reducing the magnitude of the sensor capacitance and its modulation ΔC , which are crucial for detecting the smallest particulates. The motion of PM in coplanar electrodes affect the shape of the signal to be detected. When a stream of single PM flies over the electrodes, each PM generates a single positive pulse of amplitude ΔC and width Δt (determined by the flow rate), Figure 2(d). Instead, in the PM deposition, the capacitive signal results in a rising staircase corresponding to the progressive accumulation (integral) of the particles over the electrodes, Figure 2(e). Finally, in order to cover a larger detection area, the coplanar pair can be arranged in an interdigitated structure Figure 2(c).

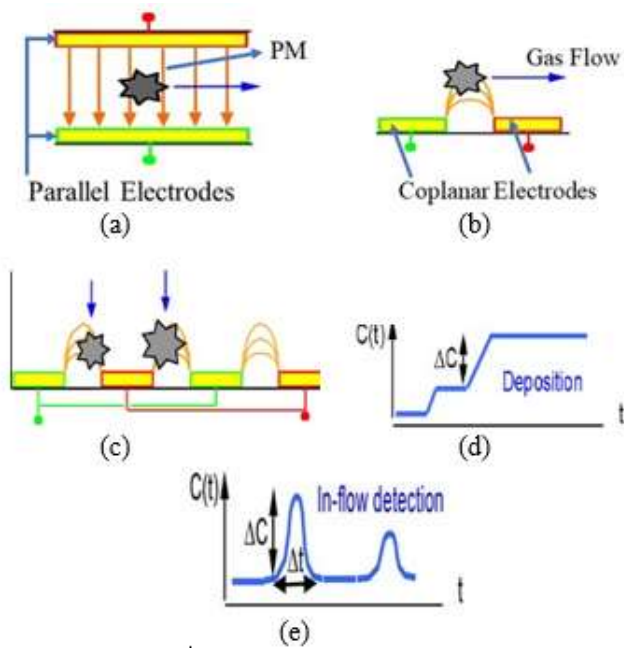


Figure 2: A proposed capacitive sensor for PM detection: possible configurations (a) Parallel-plate microelectrodes for in-flow detection of PM (b) Single coplanar pair of electrodes (c) Multiple interdigitated electrodes, an extension of (b) to provide a larger PM deposition area. (d) In flow PM detection with time (e) PM deposition measurement in terms of capacitance (Marco et al,2014).

B. Fundamental Equations

A change in capacitance with PM deposition on the sensor surface can be analyzed and related to the presented mathematical equations (Yaghouti et al, 2018).

$$E = -\nabla V \quad (1)$$

Equation (1) states the relationship between the electric field E and the electric potential V . In IDE a voltage is applied across the electrodes, creating an electric field between them.

$$D = \epsilon_0 E + P \quad (2)$$

Equation (2) is an electric displacement field equation in electromagnetism. It describes the relationship between the electric displacement field (D -measure of the electric flux density within a dielectric material), the electric field (E), and the polarization (P) of a dielectric material in the presence of an electric field.

$$-\nabla \cdot (\epsilon_0 \nabla V - P) = \rho \quad (3)$$

Equation (3) gives a modified Poisson's equation. It describes charge density ρ affects the electric potential V within the region between the interdigitated electrodes. ∇V is the gradient of the electric potential (electric potential energy per unit charge). The presence of PM determines the charge distribution ρ and the dielectric properties ϵ_0 within the region between the electrodes. The relation between C and D is implicit. To determine the capacitance of a system involving a dielectric material with PM deposits, use

equation (2) and the definition of capacitance (C) in terms of electric field and charge. The capacitance is proportional to the charges stored (Q) on the capacitor plates and inversely proportional to the voltage across the plates. For a parallel plate capacitor with a dielectric material containing PM deposited between the plates, D is expressed by equation (2). In the presence of a dielectric, the electric field inside the material is changed by a factor ϵ_0 (>1 for most dielectric materials). For PM deposits within the dielectric material, will affect ϵ_0 of the material. The presence of the PM changes the dielectric constant of the material and, consequently, the capacitance of the capacitor. A thicker PM layer decreases the effective distance between electrodes, and increased the surface area of electrodes in contact with PM leading to increased capacitance. (Yaghouti et al. 2018).

III. METHODOLOGY AND EXPERIMENTAL PROCEDURE

A. Sensor Modelling and Dimensions

The 2D Computer aided design (CAD) modelling of the sensor with the electrode is developed in COMSOL software environment as per the sensor design terminologies used in design dimensions by (Hagen et al, 2016), and optimized to get the maximum capacitance. A conventional conductometric sensor is referred to as a base for a capacitive sensor. A planer silicon substrate comprises two separated interdigitated electrodes Figure 3(a). The capacitive device could be built up with a thin but dense insulating layer covering the complete IDE area. Part of the cross-section of the capacitive sensor with IDE is shown in Figure 3(b).

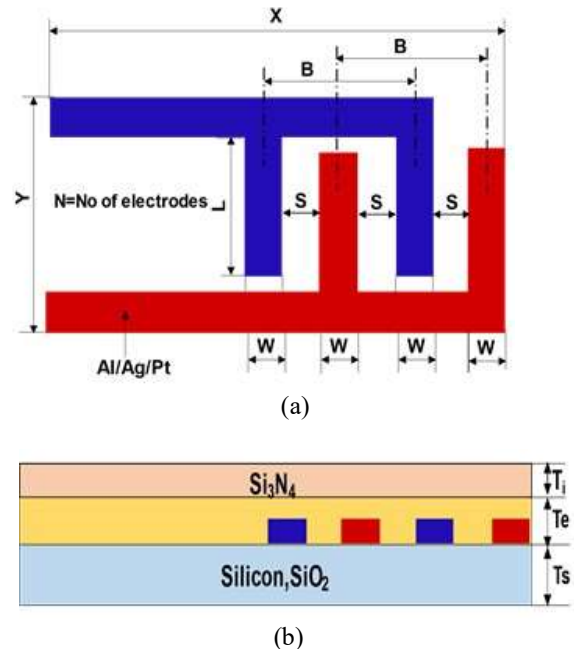


Figure 3: Interdigitated capacitive sensor (a) Structure with dimensions (b) Cross section.

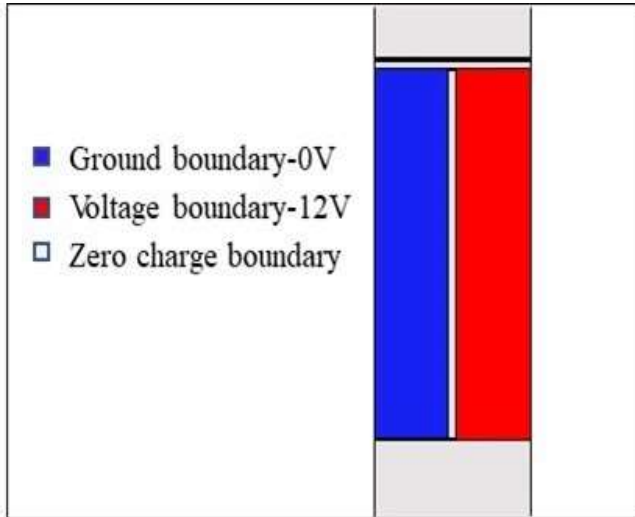
The major change in dimension was the top insulation layer thickness reduced to $5\mu\text{m}$. Details of other dimensions are provided in Table 1.

Table 1: Optimized sensor designs geometrical dimensions

Sensor Dimension	Abbreviations	Size (μm)
Electrode width	W	100
Electrode spacing	S	5
Electrode distance	B	210
Electrode length	L	4300
Insulating layer	T_i	5
Substrate Thickness	T_s	500
Substrate		
Electrode thickness	T_e	200
Number of electrodes	N	38

The sensor substrate material used is SiO_2 with a relative permittivity of 3.6, Si_3N_4 as a top insulation layer above the electrodes with 9.5 as relative permittivity, and particulates as 18.8. Gold or platinum material can be used for fabrication of electrodes. In consideration of the cost, the alumina is used for electrode material with a relative permittivity of 10.

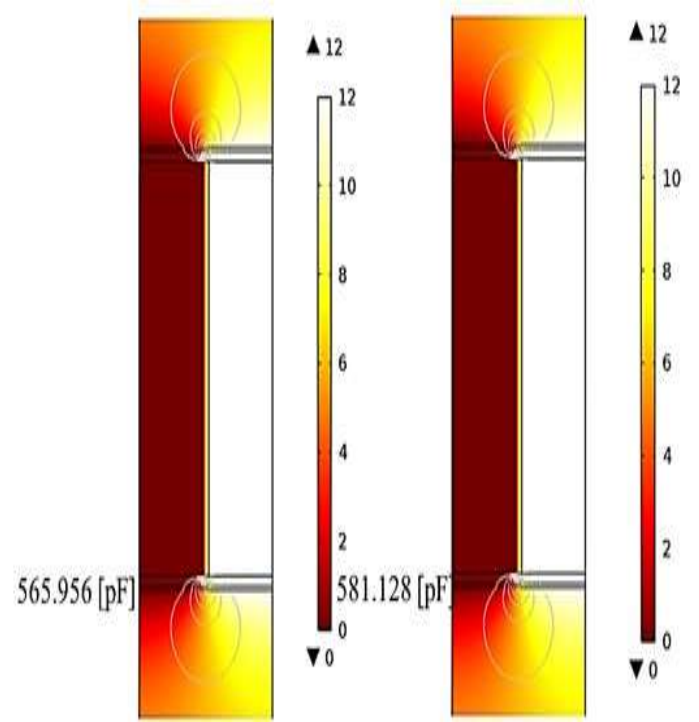
The 2D model of a single-unit cell is considered for electrostatic simulation with appropriate 3D representation. The voltage boundary, ground boundary, and zero charge boundary condition are applied to the model as shown in Figure 4. By specifying zero charges, a floating potential condition is obtained. The optimized capacitive sensor shows improved performance compared to the initial design mentioned in (Hagen et al, 2016)

**Figure 4: Interdigitated capacitive sensor boundary defined.**

B. Simulations: Extracting maximum capacitance

The electric potential field and sensor capacitance is predicted through a steady-state analysis. The Electric potential field is solved using a fully coupled direct approach. The default direct

solver for the electrostatic equations is MUMPS. Multifrontal Massively Parallel sparse direct Solver (MUMS) is a numerical solver for the solution of large sparse systems of linear algebraic equations on distributed memory parallel computers. It was developed in the European project PARASOL (1996–1999) by CERFACS, IRIT-ENSEEIH, and RAL. The electric potential magnitudes in the sensor domain with the generated capacitance magnitudes are plotted graphically in Figure 5. The PM layer thickness (T_c) varied from $0.1\mu\text{m}$ to $2\mu\text{m}$ using parametric sweep function in COMSOL. This plot is a contour plot of electric potential distribution depicting the electric field and sensor capacitance values for the optimized capacitive sensor. Similarly, the particulate diameter varied increasingly from 10nm to 100nm ($0.01\mu\text{m}$ to $100\mu\text{m}$). It shows the sensor is working properly extracting the maximum capacitance of 568pF and increasing towards 581pF . The incremental layer thickness values are converted to PM mass by using derived values from computational fluid dynamics (CFD) simulation.

**Figure 5: Surface: Electric Potential (V), Contour: Electric field, X component (V/m) for Pm Layer Thickness (T_c) from $0.1\mu\text{m}$ - $2\mu\text{m}$.**

C. Reference Sensor Modelling and Simulations: Extracting maximum capacitance

The reference sensor as mentioned in (Hagen et al, 2016), is simulated using 2D CAD modelling and applying Multiphysics (Yaghouti et al, 2018) to extract the electric field potential and capacitance generated. The sensor dimensions are mentioned in Table 2.

Table 2: Reference sensor designs geometric dimensions

Sensor Dimension	Abbreviation	Size(μm)
Electrode width	W	100
Electrode spacing	S	100
Electrode distance	B	200
Electrode length	L	4800
Insulating layer thickness	T_i	8
Substrate Thickness	T_s	635
Electrode thickness	T_e	100
Number of electrodes	N	29

Figure 6 presents the contour plots of electric potential distribution depicting the electric field and sensor capacitance values for the reference capacitive sensor. The predicted capacitance values of the sensor are matching with the experimental data with $\pm 5\%$ error (Hagen et al, 2016). The capacitance presented for the optimized sensor proved to be 10 times more than the referred sensor from the literature. The optimized sensor showed capacitance of the order of pF in the range of 500pF whereas the reference sensor was able to show a capacitance minimum of 8.40 pF and maximum up to 50 pF.

The increased resolution of the sensor provides insights that decreasing the insulation layer thickness to $5\mu\text{m}$ increases the sensitivity and resolution. Also, the $8\mu\text{m}$ as the insulating layer thickness on covering the electrodes showed no variations in the capacitance with the increase in the particulate deposition on the sensing surface. Also, the voltage applied for the optimized sensor is of the order of 12V in contrast to the reference sensor is of the order of 35V increasing to 100V.

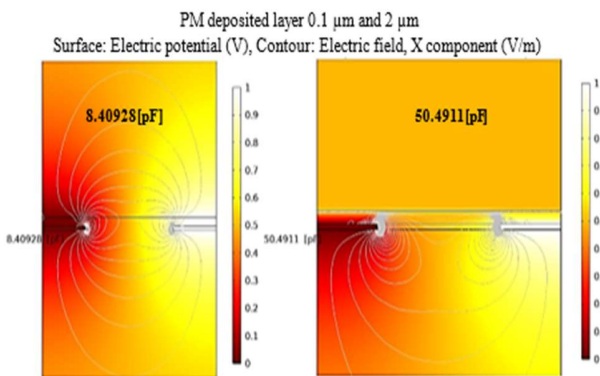


Figure 6: Reference sensor: Electric Potential (V) - Surface Plot (PM layer 0.1 μm to 2 μm).

D. Sensor Fabrication and Testing

The sensor is fabricated using thin film and lift-off technology. The fabricated device is shown in Figure 7. The fabrication process flow is shown in Figure 8. Initially, the silicon substrate undergoes a normal cleaning process with RCA1 and RCA2 solution for the removal of a foreign substrate before undergoing the oxidation process. Pyrogenic oxidation is used to create a silicon dioxide (SiO_2) layer on a silicon wafer. The SiO_2 layer can act as an insulator and the process involves exposing a material, often silicon, to high temperatures in the presence of oxygen to form a thin oxide layer. An ellipsometry technique provides the measurement of oxide layer thickness. This process may be used to create a silicon dioxide (SiO_2) layer on a silicon wafer, which can act as an insulator in a semiconductor device. Optical Lithography is used for defining patterns for IDC (Interdigitated Capacitor) on the substrate using light.

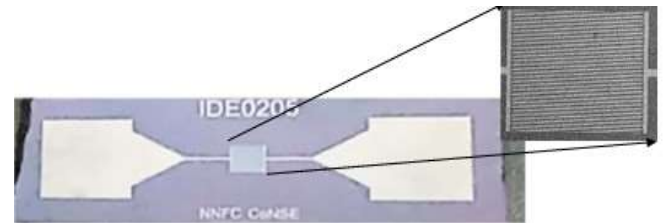


Figure 7: Fabricated device with contact pads.

Sr. No.	Process Name	Pictorial Representation
1.	RCA	
2.	Pyrogenic Oxidation	
3.	Inspection-Oxide Thickness Measurement	
4.	Optical Lithography-Pattern definition for IDC	
5.	Inspection-Microscopic Imaging	
6.	IDC Metal Deposition	
7.	Lift Off	
8.	Optical Lithography-Sensing Material	
9.	Optical Microscopic Inspection	
10.	Sensing Material Deposition	
11.	Lift Off	

Si
 SiO₂ PR
 MASK
 Si₃N₄

Figure 8: Chart presenting the sensor fabrication steps.

A desired pattern on the surface is created by applying a photoresist to the oxide layer. It is then exposed to light through a mask defining the interdigitated capacitor pattern.

The accuracy of the defined pattern was inspected through microscopic imaging. The defined pattern is covered by Aluminium deposition to form the interdigitated capacitor. A lift-off process was used to remove the excess metal that is part of the pattern. Optical lithography provides the application of a new layer of photoresist, exposed through a mask defining the sensing material pattern. After microscopic inspection to verify the accuracy of the new pattern created for the sensing material a sensing material Si_3N_4 is deposited on the substrate covering the defined electrode pattern. A lift-off process finally removes the excess material maintaining only the sensing material pattern

1. Sensor characterization and test setup

C-V characterization was conducted for the frequency range of 100 kHz to 1MHz with a voltage range of 5V. RT (resistance temperature) analysis was performed for the temperature dependency of the sensor. The temperature range used was from room temperature to 250°C. Figure 9 shows the complete setup used for CV and RT characterization

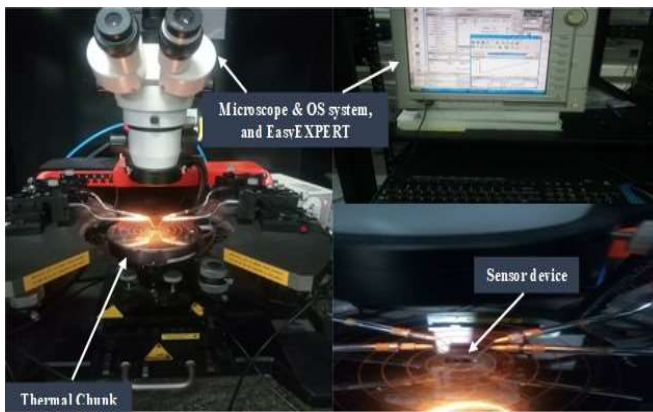


Figure 9: Experimental setup to evaluate C-V characterization DC Probe Station 1 (PM5 with Thermal Chuck, Agilent Device Analyzer B1500A).

The gas sensing test setup used is shown in Figure 10. For cross-selectivity analysis, the sensor was tested for NO_2 , CO_2 , and CO gas. It is observed that the sensor shows a selectivity of 34.29% towards other gases. A gas calibration chamber is utilized to integrate the sensor. Figure 10 shows the system, which encompasses computer-controlled measuring equipment, an electrometer from Keithley Instruments. To take real-time sensor measurements, the electrometer communicated with a computer running flow version software GPIB card from National Instruments. To introduce and release the gas, the gas detecting chamber has one inlet and outlet.

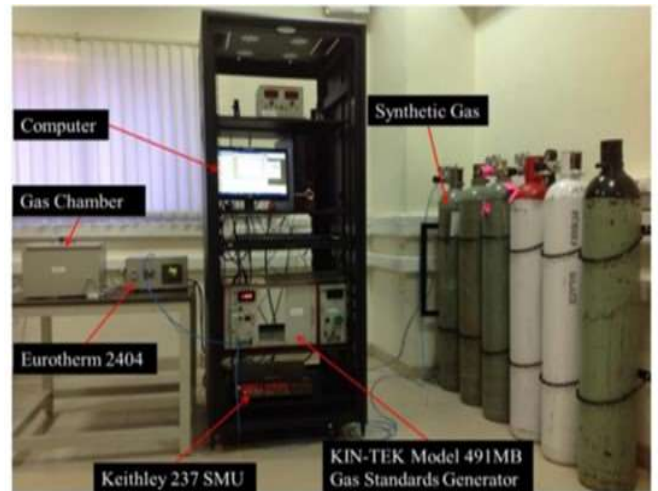


Figure 10: Gas sensing test set up for cross-sensitivity and selectivity (Shwetha et al, 2022)

2) Sensor testing on the field

Sensor testing was executed in real exhaust with the sensor surface facing the exhaust gas flow with an LCR Meter (HTC-LCR-4070). Design on experimentation (DOE) was conducted for flow velocity ranging from 35 m/s to 41 m/s and PM concentration range from $6.4\text{E}-05$ to $1.0\text{E}-06$ are considered. Sensor testing was carried out for a diesel engine model of BS-VI emission with Turbo Charged and Charged air cooled. The specifications are a capacity of 5.6 Litre, HP of 186hp@2300rpm, Max Torque of 925NM@1300rpm with speed from 32 m/s to 42 m/s for 3 min. The setup for real exhaust with the parameters mentioned is shown in Figure 11.



Figure 11: Sensor testing and validation on the field.

3) Sensor parameter characterization

The sensor parameters like sensitivity, accuracy, selectivity, and repeatability are characterized as follows (Rudraswamy et al, 2022), (Shwetha et al, 2018).

$$Sensitivity C(\%) = \frac{C_g - C_a}{C_a} \times 100 \tag{4}$$

C_a and C_g denote the capacitance of sensing film in the air and after exposure to the gas respectively. Accuracy is the measure of error rate and can be analyzed by equation (5)

$$Accuracy = 100(\%) - Error Rate \tag{5}$$

While the error rate is calculated using equation (6)

$$Error Rate(\%) = \left[\frac{Observed Value - Actual Value}{Actual Value} \times 100 \right] \tag{6}$$

Repeatability is the ability of a sensor to repeat the measurements of gas concentrations when the same input is applied to it consecutively under the same conditions. Whether to take repeatability as the standard deviation (SD) or the standard deviation of the mean (SDM), the smaller the number higher is indeed the repeatability, and the higher the reliability of the results.

$$SD(Standard Deviation) = \sqrt{\frac{\sum (X_i - \bar{X})^2}{N-1}} \text{ OR } SDM = \frac{SD}{\sqrt{N}} \tag{7}$$

Selectivity is the ability of a sensor to detect a target gas without being affected by the presence of other interference gases. Most gas sensors are sensitive to a family of gases, and it is difficult to produce a sensor specific to only one gas, it can be characterized as

$$Se(Selectivity) = \frac{C_{gas}}{C_{air}} \tag{8}$$

III. RESULTS AND DISCUSSION

A. Optimized Sensor Performance Analysis

The sensitivity analysis for different sensing parameters was analysed and the sensor presented showed maximum sensitivity for particulate deposition shown in Figure 12. Parameters like sensor dimensions and time sensitivity showed a decreasing trend. Sensor showing high sensitivity for lower mass deposition.

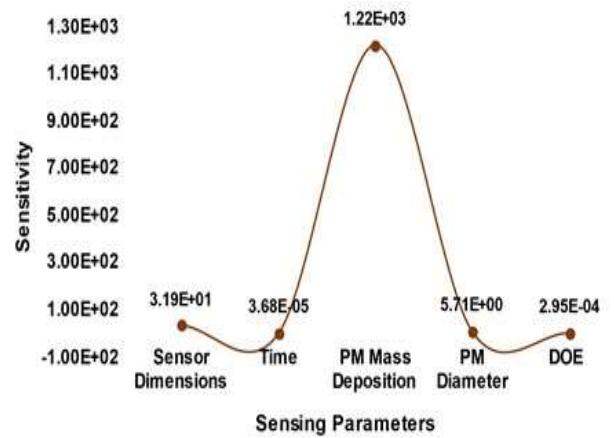
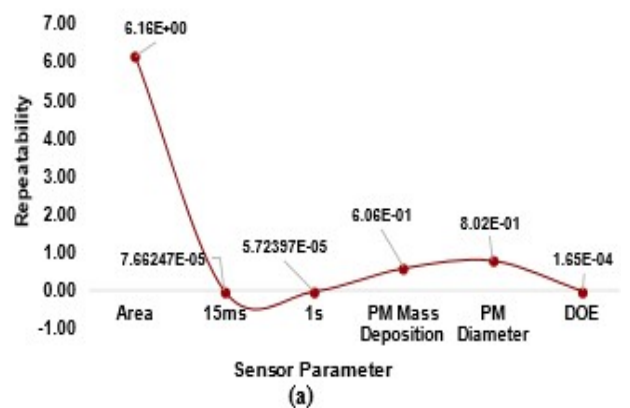


Figure 12: Analyzing sensitivity for various sensing parameters.

For other parameters like sensor dimensions and time the sensitivity showed a decreasing trend. sensor showing high sensitivity for particulate mass deposition. The repeatability of the sensor shows better for particulate deposition and increases for DOE. As per the definition from the literature (Shwetha et al, 2018) the repeatability number should be less to have a reliable sensor shown in Figure 13(a). The sensor showed high reliability for DOE at high speed and for particulate deposition. A graph in Figure 13(b) shows the highest selectivity of 65.70% for particulate deposition and 64.50% for particulate diameter. The time for deposition is considered as 15ms. The selectivity showed a decreasing trend with the increase in sensor surface area and design on experimentation (DOE). The DOE includes the varying exhaust volume from 31 m/s to 41m/s. increasing particulate disposition showing the sensor a saturated response. At this stage, the sensor needs surface cleaning known as sensor regeneration. The response time of the sensor was noted as 3.4 ms for measuring the lowest mass in mg as shown in Figure 14. The sensor response showed an exponential trend for the increase in the particulate diameter.



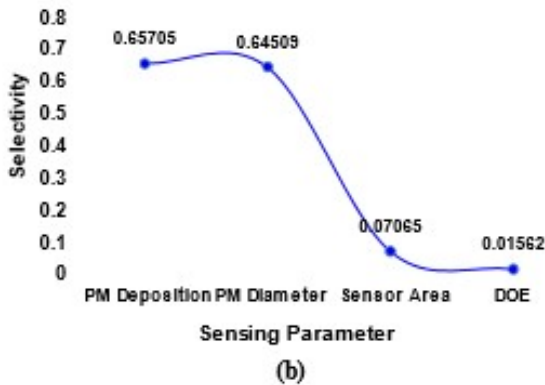


Figure 13: Optimized Sensor: Repeatability (a) and selectivity (b) for sensing parameters

The maximum capacitance obtained was 581 pF for the particulate deposition of 0.05 mg and 568.2 pF for the deposition of 0.0015 mg depicted in Figure 14. It shows the overall sensor response presenting all the operating regions. This provides valuable input to make decisions in finalizing the maintenance schedule of the particulate filter.

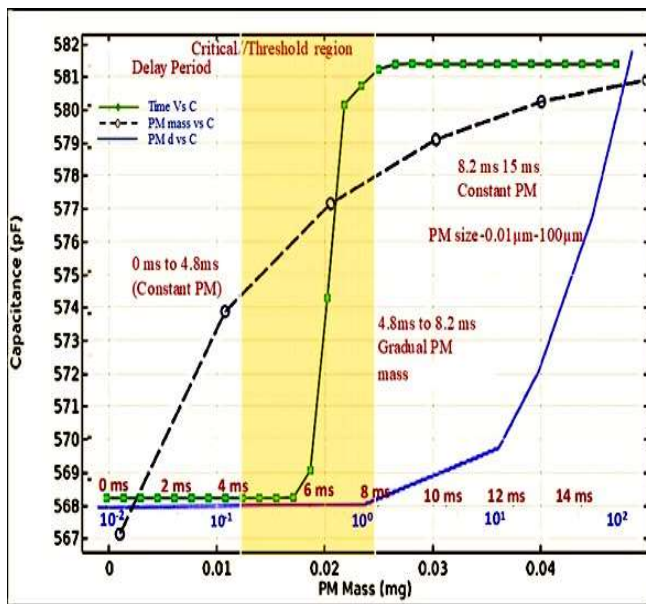


Figure 14: Overall sensor response showing all the regions.

B. Reference Sensor Performance Analysis

The measurements on the sensor were conducted in the real exhaust. The sensor was mounted with its front surface facing the exhaust gas flow. The exhaust was operated at 25% load with 1000 rpm and a pipe of 2.1.1. Distinct particulate concentrations of exhaust were applied by varying the boost pressure at a consistent pressure of 550 bar. All measurements were conducted in the real exhaust by an LCR-Meter (HP 4284A) at a frequency of 10KHz (Hagen et al, 2016). Figure 15 presents the respective maximum capacitance obtained was 42.9 pF in 180 sec with the application of 34.5 volts and 22.4 pF without an excitation.

This is in contrast to the proposed and optimized sensor, where the voltage applied was 0 to 12 V and noted the response time of 3.4 ms rather than 3 min.

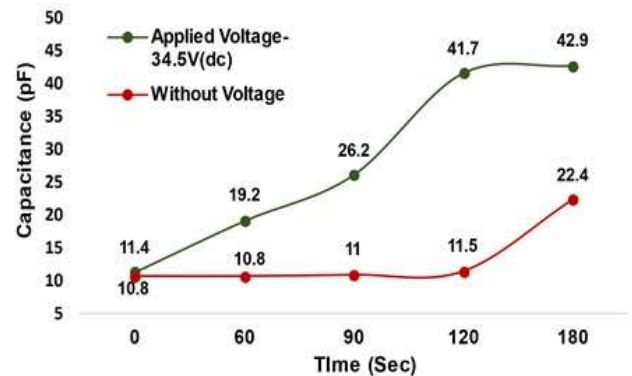


Figure 15: Reference sensor: capacitance for different time spans with and without voltage.

The measurements obtained a maximum particulate deposition of 39 mg/m³ for 74.5 kg/h and it decreases with exhaust mass flow presented in Figure 16(a) and an average selectivity of 54.55% shown in 16(b). The sensitivity obtained as 0.175 pF/Sec for a voltage of 34.5 V and 0.0644 pF/Sec without any excitation applied shown in Figure 17(a). Observed repeatability is observed as 6.36 shown in Figure 17(b), applying 34.5 V.

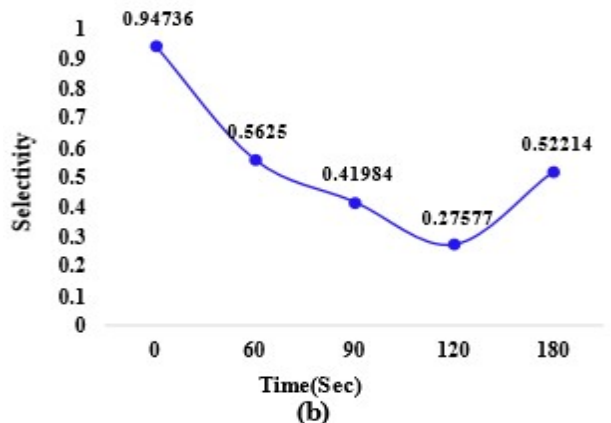
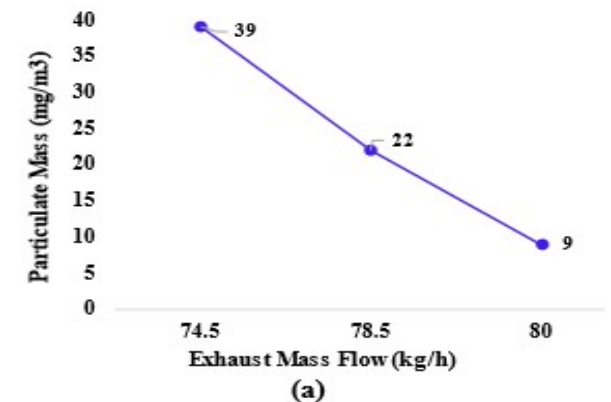


Figure 16: Reference sensor: PM deposition measurement(a) Selectivity 52.21% for 180 Sec.

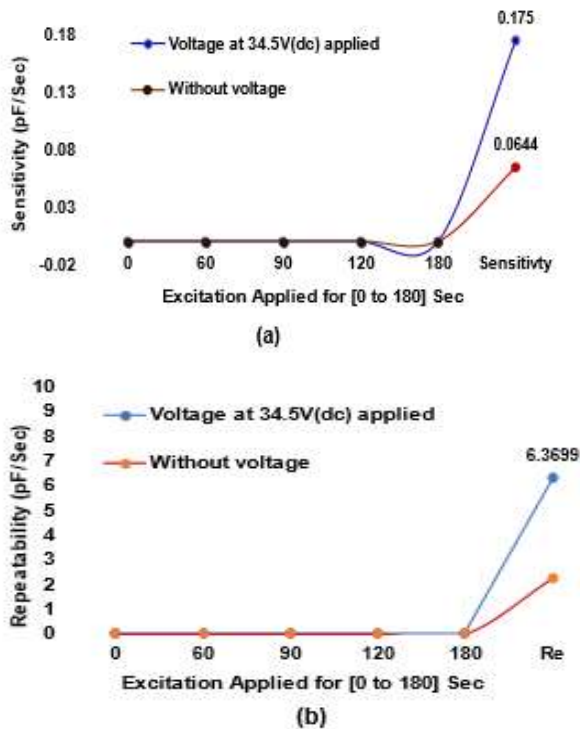


Figure 17: Reference sensor: (a)sensitivity and (b) repeatability after particulate loading for

Table 3 shows a performance comparison, of the optimized sensor and the referred sensor from the literature (Riess et al, 2016). The optimized sensor performs better than the benchmark sensor. The benchmark sensor designed with norms and a top insulating layer (Ti) of 8 μm needs high voltage to achieve capacitance resolution of the order of tens of pF. Whereas the optimized sensor was built by covering the electrode with a thin and dense insulating layer of Si_3N_4 and spacing of 5 μm . It was crucial and challenging but essential to measure small capacitance with high resolution. This change resulted reduction in applied voltage from 35 V to 12 V and high response time of 3.4 ms than 3min. The comparison shows that a well-optimized sensor shown better performance than a well-designed benchmark sensor from the literature.

Table 3: Performance comparison: Optimized Vs Benchmark Sensor

S/N	Parameter	Optimized Sensor	Benchmark Sensor
1.	Dimensions(μm)	W=100, S=5, B=210, L=4300, Ti=5, Ts=500, Te=200, N=38	W=S=100, B=200, L=4800, Ti=8, Ts=635, Te=100, N=29
2.	Max. Capacitance	581 pF	50.4911 pF
3.	Voltage applied	0-12 V	35 V
4.	Sensitivity	0.23913 pF/sec	0.175 pF/sec
5.	Repeatability	1.26 with 12 V	6.3699 with 34.5 V
6.	Selectivity	0.65705568 (65.70%)	0.54552(54.55%)
7.	Response time	0-15 ms(3.4 ms)	0-180 sec[3min]
8.	Accuracy	87.26%	64.86 %
9.	Mass Measurement	0.0045 mg/sec [0.0162 g/hr]	3.41mg/sec [12.276 g/hr]

CONCLUSION

In the present contribution, a planar capacitive particulate matter sensor was developed with optimized dimensions to improve the PM detection sensitivity. Decreasing the top insulation layer thickness and electrode spacing to 5 μm increases the sensitivity. The optimized sensor showed a maximum capacitance of 581 pF, manifolds 10 times more than the benchmark sensor [not optimized]. The sensor is highly sensitive to low mass levels and can measure a mass of 0.0045 mg/sec showing a capacitance of 568 pF. The accuracy obtained was 87.26 % as compared to benchmark sensors having 64.86% accuracy. The reference sensor measures a PM mass of 3.41 mg/sec showing a maximum capacitance of the order of 50 pF. The sensor device is also tested for cross-sensitivity using KEITHLEY 2450 Source Measure Unit (SMU)-Flow Version Software and noted as highly selective about 65.75% towards PM sensing. The study further can be extended to include the sensor regeneration facility with an inbuilt heat sink. The study provides additional input along with the Delta-P sensor to facilitate critical decision-making for particulate filter health monitoring and maintaining a plan for sensor regeneration, reducing the particulate emission to the environment.

AUTHOR CONTRIBUTIONS

V. S. KULKARNI: Formal analysis, Investigation, Methodology, Software, writing – original draft, Writing – review & editing., Data curation Validation, Resources, Conceptualization, and Funding acquisition. **S.S. CHORAGE:** Project administration, Supervision, Visualization, Writing – review & editing.

REFERENCES

- A. Sappok and L. Bromberg. (2013).** Development of Radio Frequency Sensing for In-Situ Diesel Particulate Filter State Monitoring and Aftertreatment System Control. In Internal Combustion Engine Division Fall Technical Conference, V001T04A004, American Society of Mechanical Engineers.
- A. Sappok; P. Ragaller; A. Herman; L. Bromberg; V. Prikhodko; J. Parks; J. Storey, J. (2017).** On-Board Particulate Filter Failure Prevention and Failure Diagnostics Using Radio Frequency Sensing. SAE International Journal of Engines, 10(4): 1667 - 1682.
- A.V. Mamishev; K. Sundara-Rajan; F. Yang; Y. Du. and M. Zahn. (2004).** Interdigital Sensors and Transducers. Proceedings of the IEEE, 92(5): 808 - 845.
- D. Back; D. Theisen; W. Seo; C.S.J. Tsai and D.B. Janes. (2020).** Development Of Interdigitated Capacitive Sensor for Real-Time Monitoring of Sub-Micron and Nanoscale Particulate Matters in Personal Sampling Device for Mining Environment. IEEE Sensors Journal, 20(19): 11588 – 11597.
- F. Yaghouti Niyat and M. H. Shahrokh Abadi. (2018).** COMSOL-based Modeling and Simulation of SnO_2/rGO Gas Sensor for Detection of NO_2 . Scientific Reports, 8(1): 2149.

- G. Hagen; M. Feulner; R. Werner; M. Schubert; A. Müller; G. Riess. (2016).** Capacitive Soot Sensor for Diesel Exhausts. *Sensors and Actuators B: Chemical*, 236, 1020-1027.
- H. Omran and K. N. Salama. (2015).** Design and Fabrication of Capacitive Interdigitated Electrodes for Smart Gas Sensors. Paper presented at International Conference on Smart Instrumentation, Measurement and Applications (ICSIMA2015), Kuala Lumpur, Malaysia, 1 – 4, USA: IEEE.
- H. R. Shwetha and S. B. Rudraswamy. (2018).** A Survey on Capacitive Based CO₂ Gas Sensor. *International Journal of Engineering and Technology (UAE)*, 7: 918 - 923.
- M. Carminati; L. Pedalà; E. Bianchi; F. Nason; Dubini. (2014).** Capacitive Detection of Micrometric Airborne Particulate Matter for Solid-State Personal Air Quality Monitors. *Sensors and Actuators A: Physical*, 219: 80 - 87.
- M. Feulner; F. Seufert; A. Müller; G. Hagen; R. Moos. (2017).** Influencing Parameters on the Microwave-Based Soot Load Determination of Diesel Particulate Filters. *Topics in Catalysis*, 60: 374 - 380.
- M. Feulner; G. Hagen; A. Müller; A. Schott; C. Zöllner; D. Brüggemann and R. Moos. (2015).** Conductometric Sensor for Soot Mass Flow Detection in Exhausts of Internal Combustion Engines. *Sensors*, 15(11): 28796 - 28806.
- P. Wang; Q. Lu and Z. Fan. (2019).** Evolutionary Design Optimization of MEMS: A Review of its History and State-of-the-Art. *Cluster Computing*, 22: 9105 - 9111.
- Q. Deng; L. Deng; Y. Miao; X. Guo and Y. Li. (2019).** Particle Deposition in the Human Lung: Health Implications of Particulate Matter from Different Sources. *Environmental Research*, 169: 237 - 245.
- S. D. Lowther; K.C. Jones; X. Wang; J. D. Whyatt; O. Wild; D. Booker. (2019).** Particulate Matter Measurement Indoors: A Review of Metrics, Sensors, Needs, and Applications. *Environmental Science & Technology*, 53(20): 11644 - 11656.
- S.S. Nagendra; U. Schlink; A. Müller; and M. Khare. (Eds.). (2021).** Urban Air Quality Monitoring, Modelling and Human Exposure Assessment. Springer.
- X. Hu, and W. Yang. (2010).** Planar Capacitive Sensors—Designs and Applications. *Sensor Review*, 30(1): 24 - 39.